Nanoscale

PAPER

View Article Online
View Journal

Cite this: DOI: 10.1039/c5nr09127f

Kinetics of cesium lead halide perovskite nanoparticle growth; focusing and de-focusing of size distribution†

Miriam Koolyk, Daniel Amgar, Sigalit Aharon and Lioz Etgar*

Received 22nd December 2015,
Accepted 25th January 2016

DOI: 10.1039/c5nr09127f

www.rsc.org/nanoscale

In this work we study the kinetics of cesium lead halide perovskite nanoparticle (NP) growth; the focusing and de-focusing of the NP size distribution. Cesium lead halide perovskite NPs are considered to be attractive materials for optoelectronic applications. Understanding the kinetics of the formation of these all-inorganic perovskite NPs is critical for reproducibly and reliably generating large amounts of uniformly sized NPs. Here we investigate different growth durations for $CsPbI_3$ and $CsPbBr_3$ NPs, tracking their growth by high-resolution transmission electron microscopy and size distribution analysis. As a result, we are able to provide a detailed model for the kinetics of their growth. It was observed that the $CsPbI_3$ NPs exhibit focusing of the size distribution in the first 20 seconds of growth, followed by de-focusing over longer growth durations, while the $CsPbBr_3$ NPs show de-focusing of the size distribution starting from the beginning of the growth. The monomer concentration is depleted faster in the case of $CsPbBr_3$ than in the case of $CsPbI_3$, due to faster diffusion of the monomers, which increases the critical radius and results in de-focusing of the population. Accordingly, focusing is not observed within 40 seconds of growth in the case of $CsPbBr_3$. This study provides important knowledge on how to achieve a narrow size distribution of cesium lead halide perovskite NPs when generating large amounts of these promising, highly luminescent NPs.

Introduction

Metal halide perovskites are under intense investigation for their utility in photovoltaic solar cells. The great majority of studies address the carrier transport and the long diffusion length[1,2] of bulk hybrid organic–inorganic lead halide perovskites, such as $CH_3NH_3PbI_3$, which have demonstrated a solar cell power conversion efficiency of 20.1% to date.[3] However, the nanoscale properties of the lead halide perovskites have scarcely been studied. Recently, Protesescu *et al.* reported on a novel synthesis of all-inorganic cubic cesium lead halide perovskite nanocrystals.[4] The solution process synthesis produced mono-disperse populations of colloidal $CsPbBr_3$, $CsPbI_3$, $CsPbCl_3$, and mixed halide perovskites. Follow up studies have been conducted on the ion-exchange dynamics of $CsPbX_3$ nanoparticles.[5,6] These have shown that post-synthetic treatment of $CsPbX_3$ NPs (X = Br or Cl or I) with halide donators (such as other $CsPbX_3$ NPs, lead halide salts, organo-metallic Grignard reagents, oleylammonium halides, tetrabutylammonium halides, or octadecylammonium halides) can be used to determine the final halide presence in $CsPbX_3$ NPs. This presents a post-synthetic path to spectral tuning of the nanocrystals. In addition, the original synthesis was adjusted to yield $CsPbX_3$ nanowires, and the progression of nanowire development over time was analyzed.[7] It was observed that the reactions quenched between 10 and 180 minutes after precursor injection yielded varying ratios of orthorhombic-phased nanocubes, nanosheets, and nanowires.

$CsPbX_3$ perovskites are direct bandgap semiconductors with orthorhombic, tetragonal, and cubic crystal phases, the cubic phase forming at high temperatures (above 130 °C for $CsPbBr_3$).[8] Theoretical band gap energy calculations predict band gaps of 2.00 eV and 1.44 eV for $CsPbBr_3$ and $CsPbI_3$ respectively, while experimental measurements are greater by 0.2 eV.[4] The Bohr diameter of $CsPbBr_3$ is 12 nm. Compositional alteration of the halides, as well as crystal size adjustment from the bulk, allows for optical tuning between 410 and 700 nm. $CsPbX_3$ nanocrystals have narrow emission and high quantum yields of up to 90%.[4]

The above studies demonstrate the unique and interesting properties of cesium lead halide perovskite NPs and their potential to be used in optoelectronic applications.

In this work, we study the kinetics of cesium lead halide perovskite NP growth; the focusing and de-focusing of the NP size distribution. It is important to understand the kinetics of

The Hebrew University of Jerusalem, Institute of Chemistry, Casali Center for Applied Chemistry, Jerusalem 91904, Israel. E-mail: lioz.etgar@mail.huji.ac.il

†Electronic supplementary information (ESI) available. See DOI: 10.1039/c5nr09127f

these cesium lead halide perovskite NPs in order to reproducibly and reliably generate large amounts of uniformly sized NPs. We investigate different growth durations for $CsPbI_3$ and $CsPbBr_3$ NPs, tracking their growth by high-resolution transmission electron microscopy and size distribution analysis. A model describing the kinetics of the growth is demonstrated. This study provides insight into how to successfully achieve a narrow size distribution of cesium lead halide perovskite NPs.

Experimental

Synthesis of $CsPbX_3$, X = Br, I

$CsPbBr_3$ and $CsPbI_3$ nanocrystals were synthesized according to a previously published procedure,[4] slightly adjusted. PbX_2 (99.9%), Cs_2CO_3 (99.9%), octadecene (ODE, Tech. 90%), oleic acid (OA, Tech. 90%), and oleylamine (OLA, Tech. 70%) were purchased from Sigma Aldrich. Briefly, 0.188 mmol of $PbBr_2$ or PbI_2 was dissolved in 5 mL ODE, 0.5 mL OA, and 0.5 mL OLA in a three-necked-flask, and degassed at 120 °C. 2.46 mmol (0.8 g) of Cs_2CO_3 was dissolved in 30 mL ODE and 2.5 mL OA in a three-necked-flask, and degassed at 120 °C. The Cs-oleate flask was then raised to 150 °C under argon to ensure full solubility of Cs_2CO_3. A hot syringe was used to swiftly inject 0.4 mL of the Cs precursor into the lead halide precursor solution at elevated temperatures (170 °C for Br, 145 °C for I), yielding a bright green (Br) or deep red (I) colloid. The reaction was quenched with an ice bath for 1, 4, or 40 seconds after the injection of the Cs precursor. The $CsPbBr_3$ product could be washed with hexane, precipitated by addition of isopropanol, isolated by centrifugation, and re-dispersed in hexane. The $CsPbI_3$ product was isolated directly from the ODE by centrifugation, and re-dispersed in hexane.

Absorbance measurements were performed using a JASCO V670 UV-VIS-NIR spectrophotometer.

Photoluminescence (PL) was measured using a Varian Cary Eclipse fluorescence spectrophotometer.

High resolution transmission electron microscopy (HR-TEM) and electron diffraction measurements were performed using a Tecnai F20 G2 operated at 200 kV.

PL quantum yield (PL-QY) was measured using a Hamamatsu Quantaurus-QY system.

X-ray diffraction

X-ray diffraction measurements were performed using a D8 Advance diffractometer (Bruker AXS, Karlsruhe, Germany) with a secondary graphite monochromator, 2° Soller slits and a 0.2 mm receiving slit. XRD patterns within the range of 5° to 60° 2θ were recorded at room temperature using CuKα radiation (λ = 1.5418 Å) under the following measurement conditions: a tube voltage of 40 kV, a tube current of 40 mA, step-scan mode with a step size of 0.02° 2θ and a counting time of 1–3 s per step. At GIXRD (grazing incidence X-ray diffraction), the value of the grazing incidence angle was 2.5°.

Results and discussion

In this work, we performed a detailed investigation of the impact of growth duration on product size distribution in the synthesis of all-inorganic perovskite NPs in the form of: $CsPbX_3$ where X = Br or I. Four different growth durations were studied: 1 second, 4 seconds, 20 seconds and 40 seconds. We decided to study these growth durations based on a previous observation[4] that the majority of growth of Cs lead halide NPs occurs within the first 1–3 seconds, such that we could analyze the focusing and defocusing of distribution beyond the main growth stage, between 1 and 40 seconds.

First we synthesized $CsPbBr_3$ NPs over four different growth durations: 1 s, 4 s, 20 s and 40 s. The absorbance and photoluminescence (PL) of all products exhibit a similar absorbance onset in the range of 515 nm–522 nm and a sharp photoluminescence peak in the range of 515 nm–525 nm (depends on their size) with a Full Width Half Maximum (FWHM) of 20 nm and PL-QYs of 60%. Fig. 1A shows the absorbance and PL of $CsPbBr_3$ NPs with a growth duration of 4 s compared to the absorbance of bulk $CsPbBr_3$ deposited by a one-step process[9] on the substrate (the absorbance and PL of products of the other growth durations are shown in Fig. 1S†). It can be observed that the absorbance spectra of the NPs are more pronounced than the absorbance spectra of the bulk, due to the quantum size effect in these NPs, as reported earlier.[4] The electron diffraction pattern of the $CsPbBr_3$ NPs is presented in Fig. 1B and the corresponding diffraction derived *d*-spacing is shown in Fig. 2A. The *d*-spacing match the cubic structure of $CsPbBr_3$. The XRD of the $CsPbBr_3$ NPs is presented in Fig. 2B, further supporting the cubic structure.

Fig. 3 shows the growth duration variations between 1 and 40 seconds while all other synthesis parameters were held constant. The different growth durations yielded cubic $CsPbBr_3$ NPs with an average side length of 9.0 nm for 1 second growth, 9.6 nm for 4 seconds growth, 8.4 nm for 20 seconds growth and 9.3 nm for 40 seconds growth. HR-TEM measurements can be observed in Fig. 3A–D, presenting the $CsPbBr_3$ NPs of different growth durations and the corresponding size distribution histograms (Fig. 3E–H). (The size distribution histograms were calculated from data obtained using ImageJ software, the typical analysis population being 2000 NPs.) It can be seen that the FWHM of the size distributions increases with the growth duration, implying a de-focusing process (Ostwald ripening), as discussed below.

In order to further study the variation in the size distribution of the Cs lead halide NPs, we synthesized $CsPbI_3$ NPs over four different growth durations: 1 s, 4 s, 20 s and 40 s. The absorbance and photoluminescence (PL) of all products exhibit a similar absorbance onset in the range of 695 nm−705 nm and a sharp photoluminescence peak in the range of 684 nm–695 nm (depends on their size) with FWHM of 37 nm and PL-QY in the range of 75–77%. Fig. 4A shows the absorbance and PL of $CsPbI_3$ NPs with a growth duration of 4 s (the absorbance and PL of the products of the other growth durations are shown in Fig. 2S†). The HR-TEM of a $CsPbI_3$ NP

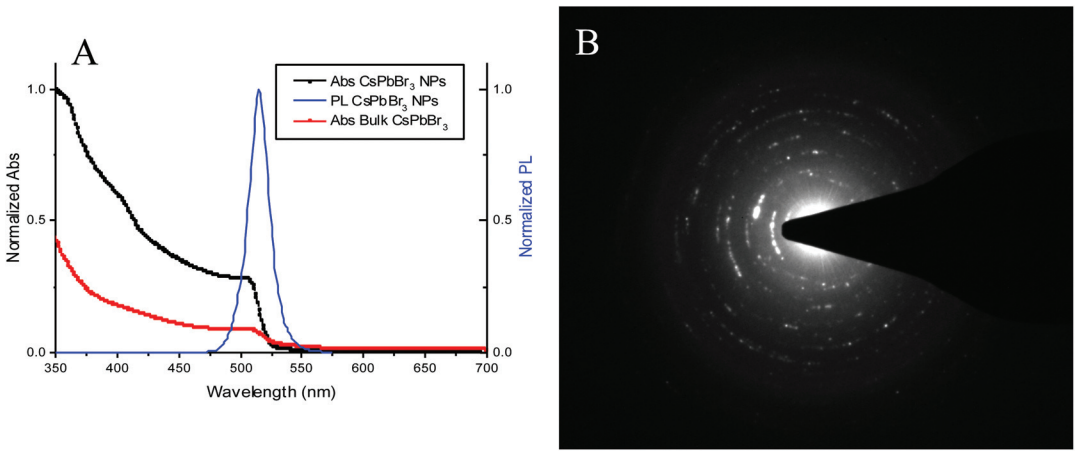

Fig. 1 (A) Absorption and photoluminescence spectra of $CsPbBr_3$, bulk and NPs at the 4 seconds growth time. (B) Electron diffraction pattern of $CsPbBr_3$ NPs.

A

d-spacing (Å)	*h*	*k*	*l*
4.14	1	1	0
2.92	2	0	0
2.07	2	2	0

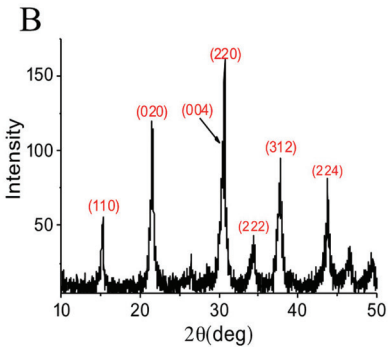

Fig. 2 (A) *d*-Spacing of $CsPbBr_3$ NPs obtained from electron diffraction and the corresponding crystal planes. (B) X-ray diffraction spectra of $CsPbBr_3$.

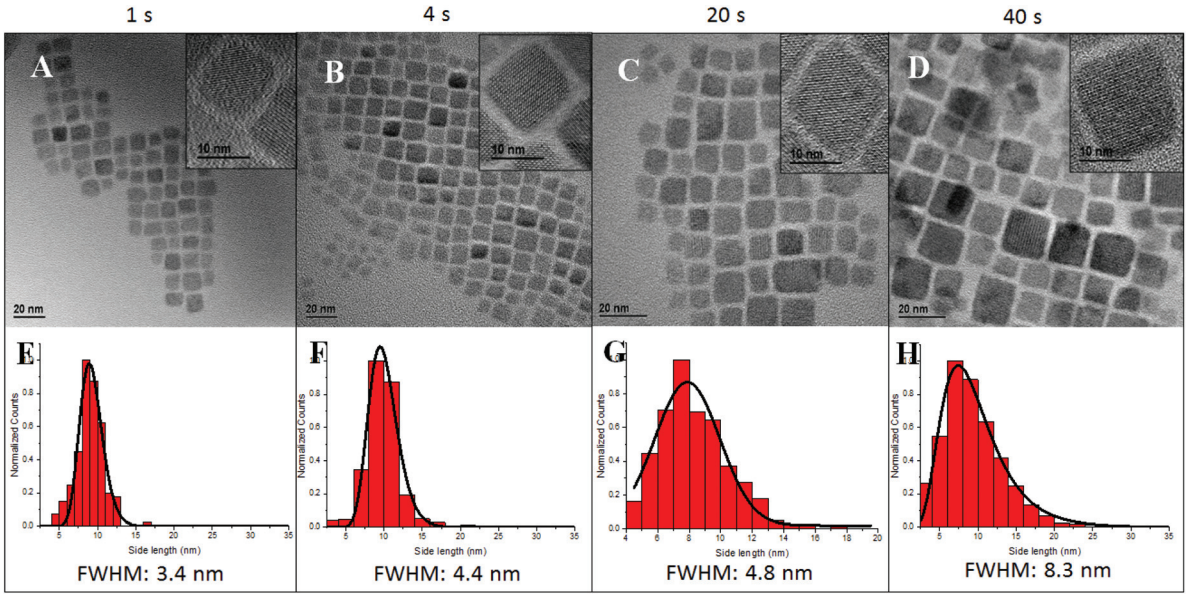

Fig. 3 HR-TEM images of $CsPbBr_3$ NPs allowed to grow for (A) 1 second, (B) 4 seconds, (C) 20 seconds, (D) 40 seconds. Inset- HR-TEM of a single NP. Normalized size distribution histograms for NP populations of each growth time; (E) 1 second, (F) 4 seconds, (G) 20 seconds, (H) 40 seconds. FWHM of the size distributions is indicated.

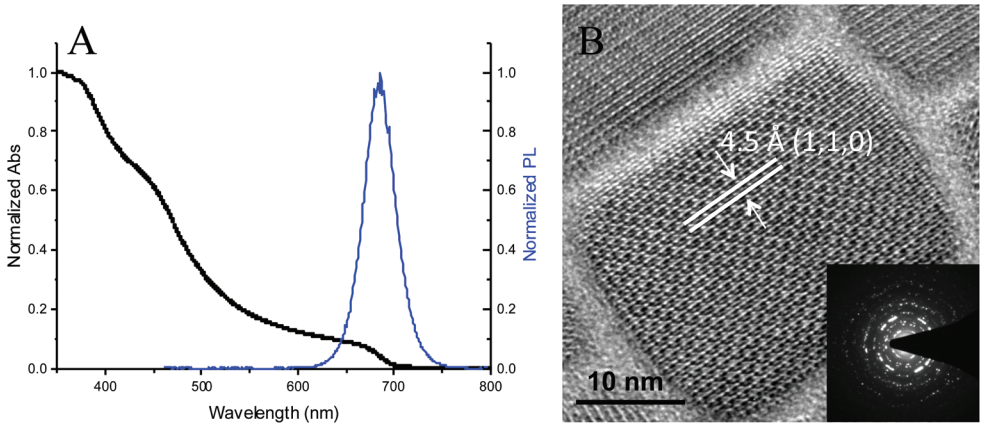

Fig. 4 (A) Absorption and photoluminescence spectra of $CsPbI_3$ NPs. (B) HR-TEM image of a particle with distinct lattice fringes and the inset of the electron diffraction pattern.

with lattice fringes is shown in Fig. 4B, corresponding to the (1,1,0) crystallographic plane. Analyzing the electron diffraction (Fig. 4B inset) provides the *d*-spacing which corresponds to the cubic crystal form of $CsPbI_3$, as detailed in Fig. 5A. The XRD of the $CsPbI_3$ NPs is presented in Fig. 5B, further supporting the cubic structure.

Fig. 6 shows the growth duration variations between 1 and 40 seconds while all other synthesis parameters were held constant. The different growth durations yielded cubic $CsPbI_3$ NPs with an average side length of 13.40 nm for 1 second growth, 10.5 nm for 4 seconds growth, 7.5 nm for 20 seconds growth and 13.46 nm for 40 seconds growth. HR-TEM measurements can be observed in Fig. 6A–D, presenting the $CsPbI_3$ NPs at different growth durations and the corresponding size distribution histograms (Fig. 6E–H). (Analysis was performed using ImageJ software.)

It can be seen that the FWHM decreases over 4 seconds and 20 seconds of growth, and increases again over 40 seconds of growth, implying de-focusing followed by focusing, followed by focusing, followed by de-focusing as will be discussed below.

As indicated above, in the case of $CsPbBr_3$, we observe the widening of the size distribution between t = 1 second and t = 40 seconds of growth duration, however in the case of $CsPbI_3$, we first observe the narrowing of the size distribution between 1 and 20 seconds of growth duration, and then the widening of the size distribution between 20 and 40 seconds.

It is expected that a burst of nucleation is followed first by a phase of distribution narrowing (focusing), and then by a second phase of distribution widening (de-focusing). The nucleation burst results in most particles being similar in size in an environment of high monomer concentration. (Monomer concentration is important because it is inversely related to the critical radius). Initially, particles smaller than the critical radius dissolve into the existing pool of monomers, while particles above the critical radius grow with a rate depending on their size: particles only slightly larger than the critical radius grow faster, while the relatively larger ones grow

A

d-spacing (Å)	*h*	*k*	*l*
4.41	1	1	0
3.12	2	0	0
2.20	2	2	0

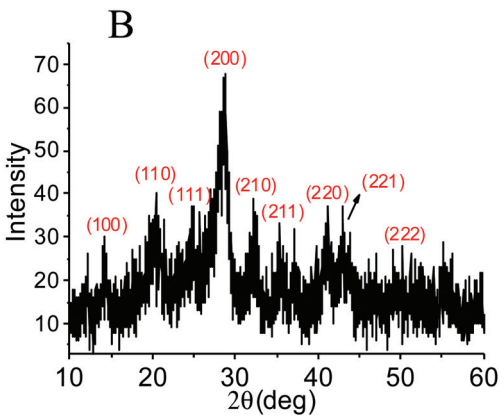

Fig. 5 (A) *d*-Spacing of $CsPbI_3$ and the corresponding crystal planes; (B) X-ray diffraction spectra of $CsPbI_3$, the XRD peaks match the crystallographic planes reported in ref. 10 and 11.

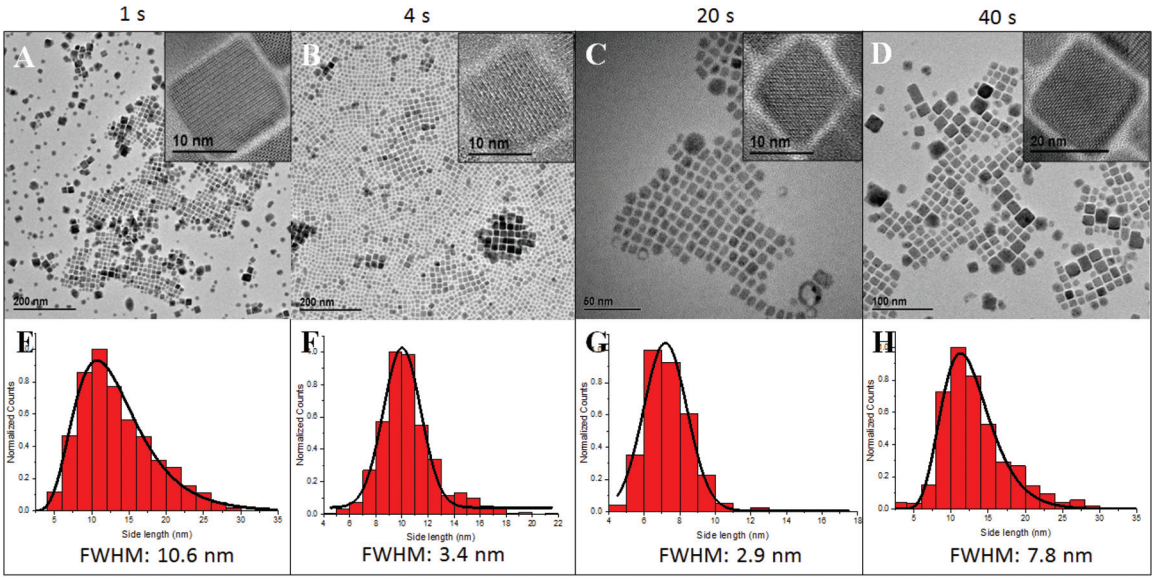

Fig. 6 HR-TEM images of $CsPbI_3$ NPs allowed to grow for times of (A) 1 second, (B) 4 seconds, (C) 20 seconds, (D) 40 seconds. Inset- HR-TEM of single $CsPbI_3$ NP at the different growth times. Normalized size distribution histograms for NP populations of each growth time (E) 1 second, (F) 4 seconds, (G) 20 seconds, (H) 40 seconds. FWHM of the size distributions is indicated.

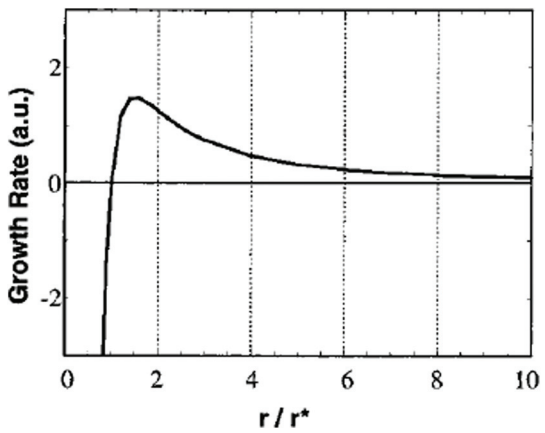

Fig. 7 The size dependent growth rate. r^* – critical radius. Reprinted with permission from ref. 12.

slower. Since particles close to the critical radius grow fastest, they "catch up" to the larger particles, bringing more of the particle population into the same size range, narrowing the distribution.[12] The size dependent growth rate is depicted graphically in Fig. 7.

When the monomer concentration is depleted as a result of growth (monomers leave the solution as they add on to growing particles), the critical radius increases past the average size. In that case, a large fraction of the population is now below the critical radius and dissolves, their monomers adding on to larger, growing particles. During focusing, most particles grow at a rate that allowed them to catch up in size to the larger particles. During de-focusing, most particles shrink/disappear while some grow, broadening the distribution. (Also named as Ostwald ripening). The formation of small particles is kinetically favored, while large particles are thermodynamically favored. However, small particles have a larger surface to volume ratio than large particles. When looking at the molecules on the surface of the particle, they are energetically less stable than the molecules in the interior of the particle. Therefore small particles will attain a lower energy state if they will transform into large particles as it happened in Ostwald ripening.

A schematic illustration of the focusing and de-focusing processes is illustrated in Fig. 8. In the case of $CsPbI_3$, we observed a moment of focusing at t = 20 seconds growth duration (stage 2 in Fig. 8), and subsequent defocusing at t = 40 seconds growth duration (stage 4 in Fig. 8). In the case of $CsPbBr_3$, only distribution widening (de-focusing) is observed (stages 3 and 4 in Fig. 8).

The main reason for the difference in the focusing/de-focusing processes between these two perovskites (*e.g.* $CsPbI_3$ and $CsPbBr_3$) is related to the monomer concentrations. As stated earlier, the monomer concentration is inversely proportional to the critical radius. The majority of growth of the Cs lead halide NPs occurs within the first 1–3 seconds, such that the growth after the first 3 seconds is mainly limited by the diffusion of the monomers. Previous reports show that the diffusion coefficient of Br is larger than the diffusion coefficient of I.[13] In addition, the synthesis temperature of the $CsPbBr_3$ NPs was higher (170 °C) than the synthesis temperature of $CsPbI_3$ (145 °C), which also suggests faster diffusion of the monomers. Therefore, it is assumed that after 4 seconds of growth the monomer concentration is more depleted in the case of $CsPbBr_3$ than in the case of $CsPbI_3$, which increases the critical radius and results in de-focusing of the population.

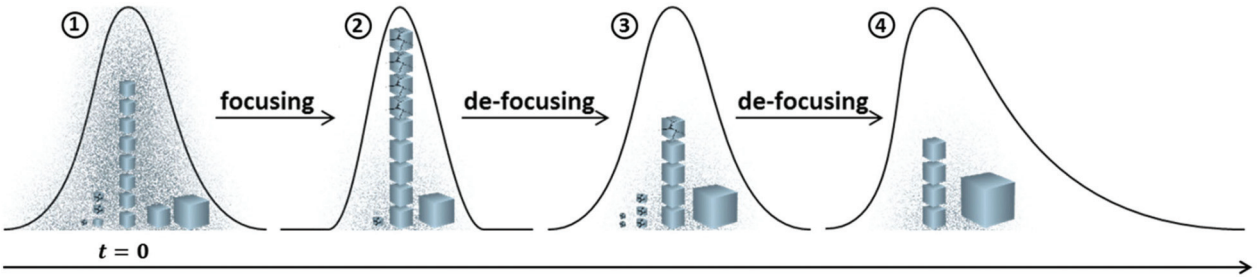

Fig. 8 Schematic illustration of the focusing and de-focusing processes. At stage 1, the reaction flask has a large population of mode-sized particles relative to that of smaller and larger particles, and the monomer concentration is high. Small particles below the critical radius dissolve into the pool of monomers while the mode-sized particles grow fast, resulting in focusing (stage 2). When the monomer concentration is depleted due to growth, the critical radius is increased and the mode-sized particles begin to dissolve, while the small population of large particles continues to grow, resulting in defocusing (stage 3). Over time, particles below the critical radius progressively dissolve while large particles progressively grow, accentuating the positive skew (stage 4).

Conclusions

In this work, we investigated the kinetics of $CsPbX_3$ (where X = Br or I) NPs as their growth durations were varied by tracking the focusing and de-focusing of the NP size distribution. In the case of $CsPbI_3$, focusing of the size distribution was observed after 20 seconds of growth duration, while further increasing the growth duration results in de-focusing of the size distribution. In the case of $CsPbBr_3$, no focusing of the size distribution was observed. The main reason for this is related to the monomer concentration, which is depleted faster in the case of $CsPbBr_3$ than in the case of $CsPbI_3$, increasing the critical radius and resulting in de-focusing of the population. To conclude, a narrow size distribution could be achieved by choosing the appropriate growth time in the case of $CsPbI_3$, while a higher monomer concentration is probably beneficial in the case of $CsPbBr_3$ in order to achieve a narrow size distribution. Understanding the kinetics of these attractive NPs is critical for their future use in optoelectronic applications.

Acknowledgements

We would like to thank Dr Inna Popov from the Center for Nanoscience and Nanotechnology at the Hebrew University of Jerusalem for performing the HRTEM micrographs. We are grateful for the financial support from the Israel Alternative Energy Foundation (I-SAEF), the Ministry of Industry Trade and Labor Office of the Chief Scientist Kamin project no. 50303, the Tashtiot project of the Office of the Chief Scientist and the young German Israel foundation grant.

References

1 S. D. Stranks, G. E. Eperon, G. Grancini, C. Menelaou, M. J. P. Alcocer, T. Leijtens, L. M. Herz, A. Petrozza and H. J. Snaith, Electron–Hole Diffusion Lengths Exceeding 1 Micrometer in an Organometal Trihalide Perovskite Absorber, *Science*, 2013, **342**, 341.

2 G. Xing, N. Mathews, S. Sun, S. S. Lim, Y. M. Lam, M. Grätzel, S. Mhaisalkar and T. C. Sum, Long-Range Balanced Electron- and Hole-Transport Lengths in Organic–Inorganic $CH_3NH_3PbI_3$, *Science*, 2013, **342**, 344.

3 http://www.nrel.gov/ncpv/images/efficiency_chart.jpg.

4 L. Protesescu, S. Yakunin, M. I. Bodnarchuk, F. Krieg, R. Caputo, C. H. Hendon, R. Xi Yang, A. Walsh and M. V. Kovalenko, Nanocrystals of Cesium Lead Halide Perovskites ($CsPbX_3$, X = Cl, Br, and I): Novel Optoelectronic Materials Showing Bright Emission with Wide Color Gamut, *Nano Lett.*, 2015, **15**, 3692–3696.

5 G. Nedelcu, L. Protesescu, S. Yakunin, M. I. Bodnarchuk, M. J. Grotevent and M. V. Kovalenko, Fast Anion-Exchange in Highly Luminescent Nanocrystals of Cesium Lead Halide Perovskites, *Nano Lett.*, 2015, **15**, 5635–5640.

6 Q. A. Akkerman, V. D'Innocenzo, S. Accornero, A. Scarpellini, A. Petrozza, M. Prato and L. Manna, Tuning the Optical Properties of Cesium Lead Halide Perovskite Nanocrystals by Anion Exchange Reactions, *J. Am. Chem. Soc.*, 2015, **137**, 10276–10281.

7 D. Zhang, S. W. Eaton, Yi Yu, L. Dou and P. Yang, Solution-Phase Synthesis of Cesium Lead Halide Perovskite Nanowires, *J. Am. Chem. Soc.*, 2015, **137**, 9230–9233.

8 C. C. Stoumpos, C. D. Malliakas, J. A. Peters, Z. Liu, M. Sebastian, J. Im, T. C. Chasapis, A. C. Wibowo, D. Y. Chung, A. J. Freeman, B. W. Wessels and M. G. Kanatzidis, Crystal Growth of the Perovskite Semiconductor CsPbBr3: A New Material for High-Energy Radiation Detection, *Cryst. Growth Des.*, 2013, **13**, 2722–2727.

9 G. E. Eperon, S. D. Stranks, C. Menelaou, M. B. Johnston, L. M. Herz and H. J. Snaith, Formamidinium lead trihalide: a broadly tunable perovskite for efficient planar heterojunction solar cells, *Energy Environ. Sci.*, 2014, **7**, 982–988.

10 Y. H. Chang and C. H. Park, First-Principles Study of the Structural and the Electronic Properties of the Lead-Halide-Based Inorganic-Organic Perovskites (CH_3NH_3) PbX_3 and $CsPbX_3$ (X = Cl, Br, I), *J. Korean Phys. Soc.*, 2004, **4**, 889–893.

11 G. Murtaza and I. Ahmad, First principle study of the structural and optoelectronic properties of cubic perovskites $CsPbM_3$ (M = Cl, Br, I), *Physica B*, 2011, **406**, 3222–3229.
12 X. Peng, J. Wickham and A. P. Alivisatos, Kinetics of II-VI and III-V Colloidal Semiconductor Nanocrystal Growth: "Focusing" of Size Distributions, *J. Am. Chem. Soc.*, 1998, **120**, 5343–5344.
13 N. Matsunaga, M. Hori and A. Nagashim, Gaseous Diffusion Coefficients of Methyl Bromide and Methyl Iodide into Air, Nitrogen, and Oxygen, *Heat Transfer—Asian Res.*, 2009, **6**, 38.